

RESEARCH ARTICLE

10.1002/2014MS000378

Self-consistency tests of large-scale dynamics parameterizations for single-column modeling

Jacob P. Edman^{1,2} and David M. Romps^{1,2}¹Department of Earth and Planetary Science, University of California, Berkeley, California, USA, ²Earth Sciences Division, Lawrence Berkeley National Laboratory, Berkeley, California, USA

Key Points:

- Self-consistency tests isolate errors due to parameterized large-scale dynamics
- WPG and WTG pass self-consistency tests based on RCE
- A new version of WPG eliminates an undesirable gravity-wave resonance

Correspondence to:

J. P. Edman,
jedman@berkeley.edu

Citation:

Edman, J. P., and D. M. Romps (2015), Self-consistency tests of large-scale dynamics parameterizations for single-column modeling, *J. Adv. Model. Earth Syst.*, 7, 320–334, doi:10.1002/2014MS000378.

Received 22 AUG 2014

Accepted 23 JAN 2015

Accepted article online 30 JAN 2015

Published online 18 MAR 2015

Abstract Large-scale dynamics parameterizations are tested numerically in cloud-resolving simulations, including a new version of the weak-pressure-gradient approximation (WPG) introduced by Edman and Romps (2014), the weak-temperature-gradient approximation (WTG), and a prior implementation of WPG. We perform a series of self-consistency tests with each large-scale dynamics parameterization, in which we compare the result of a cloud-resolving simulation coupled to WTG or WPG with an otherwise identical simulation with prescribed large-scale convergence. In self-consistency tests based on radiative-convective equilibrium (RCE; i.e., no large-scale convergence), we find that simulations either weakly coupled or strongly coupled to either WPG or WTG are self-consistent, but WPG-coupled simulations exhibit a nonmonotonic behavior as the strength of the coupling to WPG is varied. We also perform self-consistency tests based on observed forcings from two observational campaigns: the Tropical Warm Pool International Cloud Experiment (TWP-ICE) and the ARM Southern Great Plains (SGP) Summer 1995 IOP. In these tests, we show that the new version of WPG improves upon prior versions of WPG by eliminating a potentially troublesome gravity-wave resonance.

1. Introduction

Studies of idealized tropical dynamics using single-column and cloud-resolving simulations frequently incorporate parameterized large-scale dynamics to capture the interaction between the modeled domain and the environment [e.g., Chiang and Sobel, 2002; Raymond and Zeng, 2005; Kuang, 2008, 2011; Emanuel and Sobel, 2013; Bony et al., 2013]. A large-scale dynamics parameterization, also referred to as a supradomain-scale (SDS) parameterization [Romps, 2012a], diagnoses the large-scale convergence into a modeled column by comparing the modeled profile of pressure or temperature to a reference environmental profile. There are two main SDS schemes: the weak-temperature-gradient approximation (WTG) and the weak-pressure-gradient or damped-wave approximation (WPG). In the former, horizontal temperature gradients are assumed to be small, and buoyancy differences between the column and the reference environment are relaxed by vertical advection of potential temperature on some fixed time scale [Sobel and Bretherton, 2000; Raymond and Zeng, 2005; Sessions et al., 2010; Wang and Sobel, 2012; Wang et al., 2013]. On the other hand, WPG uses a parameterized form of the pressure-gradient force between the column and the reference environment to diagnose large-scale convergence [Holton, 1973; Nilsson and Emanuel, 1999; Raymond and Zeng, 2000; Kuang, 2008; Blossey et al., 2009; Kuang, 2011; Romps, 2012a, 2012b; Edman and Romps, 2014].

The goal of an SDS scheme is to produce the convergence profile that a modeled column would experience if immersed in the chosen environment. The convective dynamics within the column are modeled with either a single-column model (SCM), typically with a convective parameterization, or with a cloud-resolving model (CRM). A typical use for an SDS scheme is to feed it a time-dependent profile of temperature or pressure from observations and see whether the SCM or CRM faithfully replicates the observed precipitation. In this case, any mismatch between the observed and modeled precipitation may be due to errors in the SDS scheme, errors in the SCM/CRM, or both. Therefore, these types of simulations are not well suited for evaluating the SDS schemes.

To evaluate the SDS schemes, we need to eliminate the influence of model error. This can be accomplished by using an SCM/CRM simulation as the benchmark. Consider two simulations that use the same SCM or CRM, as depicted in Figure 1. Run 1 may, in general, be forced with any time-dependent convergence,

This is an open access article under the terms of the Creative Commons Attribution-NonCommercial-NoDerivs License, which permits use and distribution in any medium, provided the original work is properly cited, the use is non-commercial and no modifications or adaptations are made.

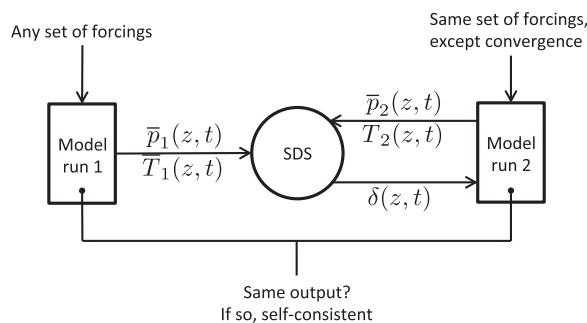


Figure 1. A general self-consistency test for an SDS scheme. An SDS scheme passes the self-consistency test if two simulations of the same SCM or CRM give the same output when forced as depicted above. In particular, run 2 is forced with the same set of forcings as run 1, except that the convergence profile is determined from the SDS scheme rather than being prescribed. In the SDS scheme, the environmental profile (either pressure for WPG or temperature for WTG) is taken from run 1.

horizontal advection, surface fluxes, and nudging. These forcings may be taken from observations or they may be constructed artificially. Run 2 uses the same set of forcings minus the convergence. Instead of being forced with a time-dependent convergence profile, run 2 uses an SDS scheme to calculate its convergence profile. And, in particular, the SDS scheme uses the temperature (for WTG) or pressure (for WPG) from run 1 as the environmental profile. Since the model used in both runs is the same, and since the forcings are identical aside from the use of the SDS scheme, any differences in the resulting model output will be due to a failure of the SDS scheme. If the model outputs are the same, then we

say that the SDS scheme has passed the self-consistency test. Here “self-consistency” refers to the model behaving the same as itself.

A more explicit example of what we mean by self-consistency is the following. Imagine a large-domain simulation of statistically steady and uniform convection. Now, consider a small subdomain. This small subdomain, if left immersed in the large-domain simulation, is unambiguously stable. If, when coupled to WTG or WPG using a reference profile representative of the larger domain, the small subdomain continues to evolve in the same statistically steady manner as it did when immersed in the large domain, then we would say that this simulation passes the self-consistency test. If the coupled simulation develops a different large-scale circulation, then the large-scale dynamics parameterization is not faithfully representing the interaction between the smaller subdomain and the large-scale environment. We would say, in this case, that the SDS scheme fails the self-consistency test.

In particular, we will say that an SDS scheme passes the self-consistency test if it generates domain-mean anomalous ascent or descent that is much smaller in magnitude than the radiatively driven clear-sky descent speed in the benchmark simulation. For example, an SDS scheme that perfectly replicates an RCE benchmark will have a domain-mean ascent profile that is zero; since zero is certainly less than $O(0.1)$ of the radiatively driven clear-sky descent speed, this SDS is self-consistent. On the other hand, if the SDS scheme causes the atmosphere to dry out and descend en masse to balance radiative cooling, then the domain-mean descent speed will be comparable to the clear-sky descent speed in the benchmark RCE simulation; therefore, this SDS scheme would be considered to have failed the self-consistency test in spectacular fashion.

Much of the work using single-column and cloud-resolving models coupled to large-scale dynamics parameterizations has focused on the conditions leading to multiple equilibria (i.e., the presence of distinct wet and dry equilibrium states) [Sobel *et al.*, 2007; Sessions *et al.*, 2010] or on comparisons with observations [e.g., Wang *et al.*, 2013]. There has been comparatively little effort expended on studying whether or not commonly used SDS schemes can simply reproduce the behavior of a model immersed in a larger version of itself. This is the goal of the self-consistency tests we conduct in this study. In order to reliably compare model results with observations, one might reasonably expect that an SDS scheme must be able to pass a self-consistency test. Some implementations of WTG have been shown to fail self-consistency tests [Raymond and Zeng, 2005; Raymond, 2007; Daleu *et al.*, 2012], and Kuang [2011] found that one implementation of WPG passes for some parameter choices, but not others.

But, is it fair to expect these SDS schemes to succeed in these self-consistency tests? What if failing a self-consistency test simply reflects a true instability in convecting atmospheres, whereby a statistically uniform patch of atmosphere evolves a large-scale circulation? Indeed, it has been suggested that the existence of multiple equilibria in single-column models with an SDS scheme is related to the phenomenon of convective aggregation [Sobel *et al.*, 2007]. Fortunately, we can exclude this possibility so long as we use fixed radiative cooling profiles in the self-consistency tests. Although convective aggregation has been studied extensively in numerical models [Held *et al.*, 1993; Bretherton *et al.*, 2005; Stephens *et al.*, 2008; Muller and

Held, 2012; Jeevanjee and Romps, 2013; Emanuel et al., 2014; Wing and Emanuel, 2014], there has been no example of convective aggregation with fixed, horizontally uniform radiative cooling. In fact, all indications are that interactive radiation (i.e., radiation that interacts with water vapor and clouds) is essential to the triggering and maintenance of convective aggregation. Therefore, when using fixed radiation, SDS schemes should be able to pass self-consistency tests.

A key motivation for this study is to test the new form of WPG introduced by Edman and Romps [2014] in a cloud-resolving framework. In that study, we used an idealized shallow-water framework to show that the new WPG improves upon previous implementations of WPG and WTG by more accurately capturing steady state and transient dynamics. Additionally, in the idealized system, this new form of WPG removes a potentially troublesome gravity-wave resonance found in prior versions of WPG. In such a case, rather than damping the buoyancy anomaly away on the time scale for gravity-wave emission from the column, the column coupled to old WPG behaves as though an infinite, convectively coupled wave is passing through the domain [Romps, 2012a]. This behavior is undesirable if one is attempting to parameterize the interaction between convection and large-scale convergence. In this study, we present evidence that this gravity-wave resonance can cause problems in simulations coupled to WPG and show that it is eliminated entirely in the new WPG presented by Edman and Romps [2014].

In this paper, we use cloud-resolving simulations with and without large-scale dynamics parameterizations to test the claims of improvement to WPG made by Edman and Romps [2014] using self-consistency tests. First, we perform self-consistency tests with WPG and WTG using a cloud-resolving model in a simple radiative-convective equilibrium (RCE) framework. We also perform self-consistency tests with observed forcings, by comparing simulations forced with vertical-velocity observations from two observational campaigns—the Tropical Warm Pool International Cloud Experiment (TWP-ICE) [Fridlind et al., 2010] and the Atmospheric Radiation Measurement (ARM) Southern Great Plains (SGP) intensive observational period (IOP) of July 1995 [Ghan et al., 1999]—with simulations using large-scale dynamics parameterized by new WPG, old WPG, and WTG. Section 2 describes the implementations of the three large-scale dynamics parameterizations used in this study (2 versions of WPG, 1 version of WTG). Section 3 describes the RCE self-consistency tests and contains a brief discussion of their implications. In section 4, we describe the self-consistency tests based on the TWP-ICE and SGP data and discuss the gravity-wave resonance problem in old WPG. We conclude with a brief discussion in section 5.

2. Implementations of WPG and WTG

The SDS scheme that we refer to as “old WPG” is the version used in Romps [2012b]. The horizontal divergence $\delta(z,t)$ is calculated by

$$\partial_t \delta(z, t) = \frac{1}{L^2} \frac{\bar{p}(z, t) - p_0(z, t)}{\bar{\rho}(z, t)} - \alpha^* \delta(z, t), \quad (1)$$

where the overbar represents the horizontal average over the column and a subscript 0 denotes the environmental reference profile that is provided to the parameterization. The length scale L and time scale $1/\alpha^*$ are input parameters to the scheme.

“New WPG” is a modification to old WPG introduced by Edman and Romps [2014], in which equation (1) is replaced by the following pair of equations:

$$\partial_t \delta'(z, t) = \frac{1}{L^2} \frac{\bar{p}(z, t) - p_0(z, t)}{\bar{\rho}(z, t)} - \alpha^* \delta'(z, t), \quad (2)$$

$$\delta(z, t) = \delta'(z, t) + \frac{2\pi L}{HN} \partial_t \delta'(z, t). \quad (3)$$

Here the horizontal divergence $\delta(z,t)$ is the old WPG divergence $\delta'(z, t)$ modified by a term proportional to the length scale L divided by the first-baroclinic wave speed NH/π (i.e., the time for a dry first-baroclinic wave to cover a distance L), where N is a reference Brunt-Väisälä frequency and H is the height scale. This factor is added to account for the back reaction exerted on a column of fluid by gravity waves exiting the column, as described in Edman and Romps [2014].

We implement WTG in the relaxed form following *Raymond and Zeng [2005]*, where the vertical velocity $w(z, t)$ is calculated as

$$w(z, t) = \frac{\bar{\theta}_v(z, t) - \theta_{v0}(z, t)}{\tau \max[\gamma, \partial_z \theta_{v0}(z, t)]}, \quad (4)$$

above a height of 1 km. Below $z = 1$ km, w is linearly interpolated to zero at the surface. A minimum stability of $\gamma = 0.01 \text{ K km}^{-1}$ is enforced in the denominator to avoid singularities, and τ is a relaxation time scale that is an input parameter to the scheme. This vertical velocity is then converted to a horizontal divergence $\delta(z, t)$ by

$$\delta(z, t) = -\frac{1}{\bar{\rho}(z, t)} \partial_z [\bar{\rho}(z, t) w(z, t)]. \quad (5)$$

The horizontal divergence calculated by an SDS scheme defines a mass source, $-\rho\delta$, which is added to the cloud-resolving model's tendencies of density, water vapor, and temperature. Following *Romps [2012b]*, we also include the horizontal advective effect of convergence over the modeled domain in the tendencies of potential temperature and water vapor. This is represented by a second-order centered method, such that the tendency equations have the following modifications:

$$\partial_t \rho(\mathbf{x}, t) = -\rho(\mathbf{x}, t) \delta(z, t) + \dots, \quad (6)$$

$$\partial_t [\rho(\mathbf{x}, t) q_v(\mathbf{x}, t)] = -\rho(\mathbf{x}, t) \delta(z, t) \left\{ q_v(\mathbf{x}, t) + \frac{1}{2} [q_{v0}(z) - q_v(\mathbf{x}, t)] \right\} + \dots, \quad (7)$$

$$\partial_t [\rho(\mathbf{x}, t) \theta(\mathbf{x}, t)] = -\rho(\mathbf{x}, t) \delta(z, t) \left\{ \theta(\mathbf{x}, t) + \frac{1}{2} [\theta_0(z) - \theta(\mathbf{x}, t)] \right\} + \dots \quad (8)$$

Note that the above equation for potential temperature θ was incorrectly written in terms of absolute temperature in *Romps [2012b]*, but it was correctly implemented in terms of potential temperature both there and here.

All simulations are performed using the fully compressible, cloud-resolving model Das Atmosphärische Modell (DAM) [*Romps, 2008*] with 2 km grid spacing in the horizontal, a doubly periodic domain, and no Coriolis force. The vertical grid is stretched, ranging from approximately 50 m grid spacing near the surface up to 1 km near the model top, which is at 32 km.

3. Self-Consistency in RCE

Radiative-convective equilibrium (RCE) is a state of no mean convergence into the simulated column, and it serves as a particularly simple situation in which to test self-consistency. We use the following basic procedure for the self-consistency tests: (1) run a cloud-resolving model to RCE with fixed SST and fixed radiative cooling, without any SDS scheme; (2) run an identical simulation, but coupled to either WPG or WTG, using the mean profiles of pressure (for WPG) or temperature (for WTG) from the first simulation as the reference environment. These two steps correspond to model runs 1 and 2 in Figure 1. If the SDS scheme passes the self-consistency test, run 2 should exhibit no mean ascent.

For both runs 1 and 2, surface fluxes are calculated using a bulk aerodynamic formula over an ocean with a fixed SST of 300 K and the profile of radiative cooling is fixed as the average of an otherwise identical 120 day RCE simulation with interactive radiation. Run 1 lasts 240 days; run 2 is initialized from a 3-D snapshot taken at the end of the run 1, and it lasts 90 days. The reference profiles of temperature, pressure, and water vapor used as input to the SDS schemes in run 2 are averages over the last 120 days of run 1.

Self-consistency in RCE appears to depend on the choice of relaxation parameter for each scheme (e.g., τ for WTG and L for both WPGs). We test three choices of relaxation parameter for each scheme, corresponding to different adjustment time scales (τ) for WTG and different length scales (L) for WPG. The three values of L are 128, 1280, and 12,800 km. The smallest value of L is twice the width of the domain and the largest is $\approx 1/3$ the circumference of the earth at the equator. For WTG, τ is set to L/c , where $c \approx 50 \text{ m s}^{-1}$ is the approximate wave speed of the first baroclinic mode in the tropical atmosphere, so τ takes the values

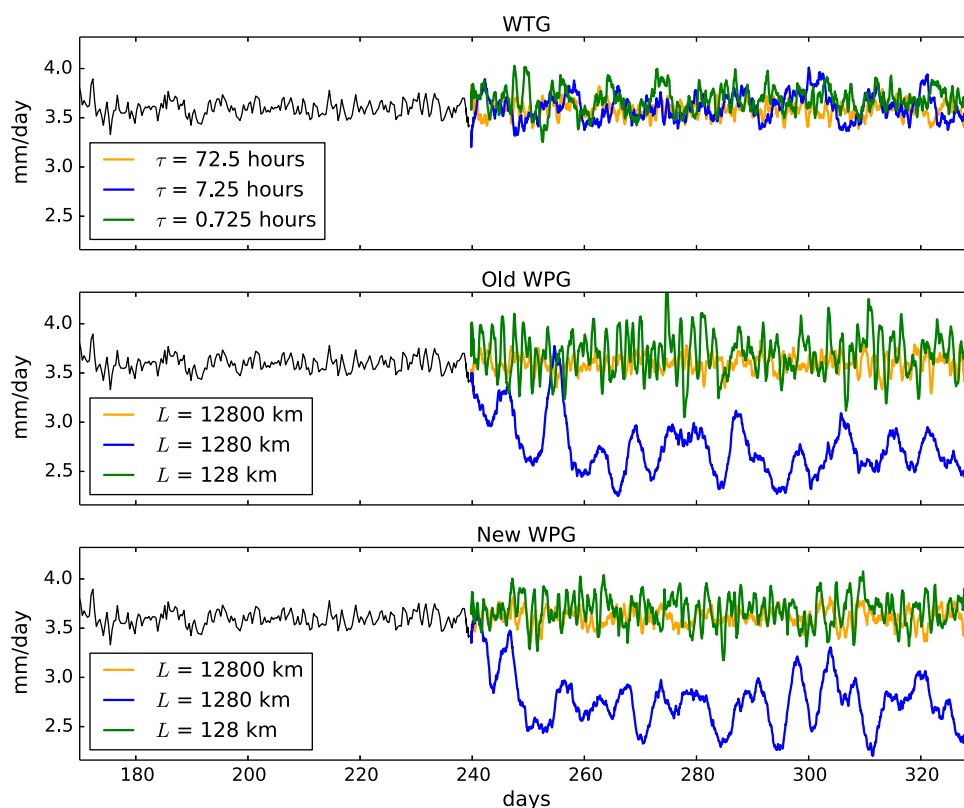


Figure 2. Rainfall time series for the RCE self-consistency tests. In all plots, the thin black line depicts the domain-averaged precipitation from the RCE simulation. The results of the coupled simulations ((top) WTG; (middle) old WPG; (bottom) new WPG) are shown after day 240; the green lines represent the precipitation from simulations with the strongest coupling to WPG or WTG (e.g., $L = 128$ km for WPG, $\tau = 0.725$ h for WTG), the blue lines show the intermediate choice, and the orange lines show the case with the weakest coupling, which is effectively RCE for all the SDS schemes.

0.725, 7.25, and 72.5 hours. Additional simulations (not shown) with a larger domain (144×144 km) indicate that WTG may become more self-consistent with larger domain sizes, while WPG is much less sensitive.

Figure 2 shows the precipitation time series from the last part of run 1 (RCE) and the entirety of run 2 (the SDS parameterized simulations) for each choice of SDS scheme and relaxation parameter. Run 2 begins at day 240 and continues until day 330; thick, colored lines show results for WTG (top), old WPG (middle), and new WPG (bottom). For all SDS schemes with the parameter choice corresponding to the slowest adjustment (e.g., $\tau = 72.5$ h and $L = 12,800$ km; orange lines in Figure 2), the precipitation time series for run 2 is nearly indistinguishable from the RCE in run 1 (thin black lines). In those cases, the parameterized adjustment is so weak that the column is effectively decoupled from the environment.

For $L = 1280$ km, both new and old WPG exhibit oscillatory behavior on a ≈ 10 -day time scale, similar to that seen in Kuang [2011], and there is less mean precipitation than in the RCE run. The 10-day oscillation and most of the change in the mean disappears for $L = 128$ km, but larger variability on shorter time scales remains (although this is somewhat reduced for new WPG relative to old WPG). For both choices of τ , WTG appears more similar to the RCE case than any of the versions of WPG. There is almost no change in the mean precipitation relative to the RCE case, but the case with $\tau = 7.25$ h has a ≈ 10 -day period oscillation similar to both versions of WPG, albeit with smaller amplitude. Note that this 10 day oscillation is distinct from the gravity-wave resonance discussed previously; it is not possible for the gravity-wave resonance to occur in WTG or new WPG. Also, the p and w anomalies are in phase for 10-day period oscillations, in contrast to the gravity-wave resonance where the p and w anomalies are in quadrature.

Figure 3 shows the resulting vertical-velocity profiles for each of the “run 2” simulations, averaged over the full 90 days. For a large-scale dynamics parameterization that is perfectly self-consistent, the mean vertical-velocity profile would be zero at all heights, i.e., the same as the RCE state. This requirement is very closely

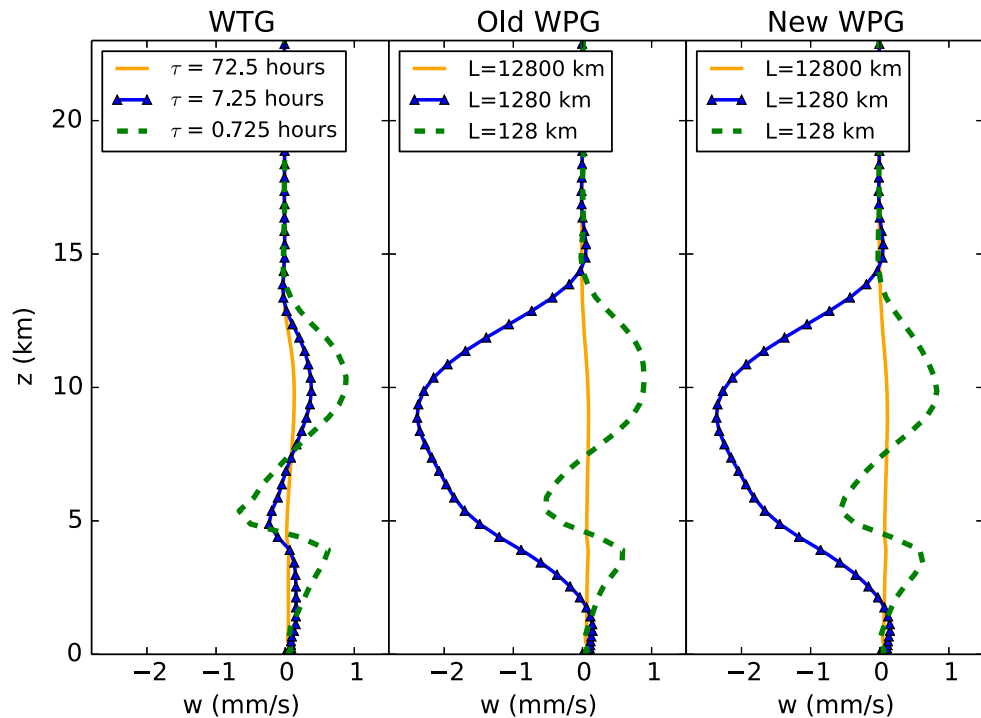


Figure 3. The 90 day mean profiles of vertical velocity from RCE self-consistency tests for each of the large-scale dynamics parameterizations (left) WTG; (middle) old WPG; (right) new WPG for three parameter choices (see legend).

met in the cases of $\tau = 72.5$ h and $L = 12,800$ km; these parameters are planetary scale, so that the coupling to large-scale dynamics is so weak that it has a negligible effect on the modeled convection and the column is actually in RCE. For other values of L and τ , there are noticeable deviations of the vertical-velocity profiles from zero; these deviations will be compared to the radiatively driven descent speeds below. As expected, the mean vertical-velocity profiles for new and old WPG are nearly identical; the two schemes only differ in their treatment of transient disturbances.

One striking feature of these simulations is the agreement between WPG and WTG for small L and τ ; for $L = 128$ km and $\tau = 0.725$ h, the vertical-velocity profiles are almost identical, with strongly third-baroclinic structure. This agrees with the findings of Kuang [2012], who found that simulations of atmospheric circulations over SST hotspots using WTG and WPG converge to a similar third-baroclinic structure [see Kuang, 2012, Figures 10 and 11] in the limit of small L and τ . It is notable that this same structure persists in our RCE self-consistency tests, in the absence of any SST anomaly.

On the other hand, WTG and WPG exhibit very different behavior as the relaxation parameter is increased. For WTG, increasing τ reduces the mean vertical motion, which decreases monotonically toward zero until the column is in RCE (e.g., the simulations with $\tau = 72.5$ h). This agrees with the findings of Daleu *et al.* [2012], although their model had descending motion for all values of τ ; clearly some aspects of this circulation are dependent on the model setup, although the parameter dependence seems robust. In contrast, the vertical motion in the WPG simulations does not monotonically decrease toward zero as L is increased. When L is increased from 128 to 1280 km, the third-baroclinic structure in the vertical-velocity profile disappears, and is replaced by first-baroclinic descent with more than twice the magnitude. But, as L is increased further, the column does in fact approach RCE (e.g., the WPG simulations with $L = 12,800$ km). The WPG simulations of Kuang [2012] also show this tendency toward deeper structure for larger L , but the nonmonotonic approach to RCE is a novel feature of these simulations.

Although these nonzero vertical-velocity profiles tell us that WTG and WPG are not perfect, are they “good enough” for practical use? Our criteria for passing a self-consistency test—that the vertical-velocity errors are small compared to radiatively driven clear-sky subsidence—is designed to answer this question. The net radiative cooling rate of the troposphere is equal to about 1 K d^{-1} . The subsidence rate is given by

$w = gQ/N^2T$, where N is the Brunt-Väisälä frequency and Q is the radiative cooling rate in dimensions of Kelvin per time. Using values realistic for the mid-troposphere, this results in $w \approx -4 \text{ mm s}^{-1}$. For all three values of τ , the domain-mean w in the WTG simulations is $\leq 1 \text{ mm s}^{-1}$, which is much smaller in magnitude than $\approx 4 \text{ mm s}^{-1}$, so we conclude that WTG passes these self-consistency tests. The story is a bit different, however, for WPG. For small and large L (128 and 12,800 km), the WPG profiles are nearly identical to the WTG profiles for small and large τ (0.725 and 72.5 h), and they meet the requirement for self-consistency. For intermediate L (1280 km), however, the WPG profile takes a value of about -2 mm s^{-1} , which is comparable to the radiatively driven clear-sky descent speed of about -4 mm s^{-1} . For intermediate L , therefore, we conclude that new and old WPG do not pass these self-consistency tests. In the next section, we perform self-consistency tests with observed forcing, which emphasizes the ability of each SDS scheme to deal with transient disturbances.

4. Self-Consistency With Observed Forcings

We adapted case studies from two observational campaigns focused on single-column model intercomparisons: the Tropical Warm Pool International Cloud Experiment (TWP-ICE) [Fridlind *et al.*, 2010] and the July 1995 intensive observation period (IOP) at the ARM Southern Great Plains site [Ghan *et al.*, 1999]. However, rather than use the observed environmental reference profiles to drive WPG and WTG [e.g., as in Wang *et al.*, 2013], we “filter” the observations through a benchmark simulation forced with the observed vertical velocity, and then use the pressure and temperature profiles from the benchmark simulation as input to WPG and WTG. This is the same procedure depicted in Figure 1. This self-consistency test allows for a direct comparison between the benchmark and SDS-enabled simulations without contamination from any model or observational errors other than those introduced by the SDS scheme itself.

For the time-varying self-consistency tests, we use a 128 km square domain. The benchmark simulation is forced with the observed large-scale vertical velocity from observations. The simulations with parameterized large-scale dynamics derive their own vertical velocity using time-varying reference profiles taken from the benchmark simulation. Because WPG and WTG have been shown to respond strongly to variations in surface fluxes [Wang *et al.*, 2013], but we are mainly interested in their ability to produce convergence profiles consistent with heating anomalies in the column, we use time-invariant surface and advective forcings and noninteractive (but time-varying) radiative cooling profiles for both the benchmark and WPG/WTG-coupled experiments.

Additionally, all simulations are initialized using observed profiles of wind, temperature, and humidity; the temperature field is perturbed with 0.01 K noise in the first layer of the domain. Parameters for new and old WPG are set following Edman and Romps [2014], with $L = 128 \text{ km}$ (the size of the domain) and $\alpha^* = \alpha(1/3 + r/2)$, where $1/\alpha$ is the Rayleigh damping time scale for the troposphere, taken here to be 5 days. The value of r is not well constrained (see discussion in Edman and Romps [2014]), but it represents the ratio of the size of the region affected by anomalous convection in the modeled column to the size of the anomalously convecting column; here we set $r = 10$. For new WPG, we set the factor $2\pi/HN = 0.042 \text{ s m}^{-1}$, corresponding to $H = 15 \text{ km}$ and $N = 0.01 \text{ s}^{-1}$. For WTG, we set τ as the time for a first baroclinic wave to traverse the domain $\tau = 128 \text{ km}/49 \text{ m s}^{-1} = 0.725 \text{ h}$, which is comfortably within the range established by previous studies [e.g., Cohen and Craig, 2004; Wang and Sobel, 2011; Wang *et al.*, 2013].

4.1. TWP-ICE

For the TWP-ICE self-consistency test, the surface fluxes and radiative cooling profile for the benchmark and WPG/WTG runs are taken from a simulation identical to the benchmark simulation (prescribed observed vertical velocity), but with surface fluxes calculated interactively using the bulk aerodynamic formula over an ocean with SST fixed at the observed mean of 302 K, and radiation calculated interactively every 10 minutes. To assess the relative performance of WTG, old WPG, and new WPG, we compare the precipitation time series from each simulation with parameterized large-scale dynamics against the precipitation time series from the benchmark simulation. Precipitation is a relatively holistic way to assess performance, because it is closely related to the large-scale convergence produced by the SDS scheme.

The resulting precipitation time series are shown in Figure 4. WTG, old WPG, and new WPG are shown in the top, middle, and bottom plots, respectively. In all three plots, the result of the benchmark simulation is

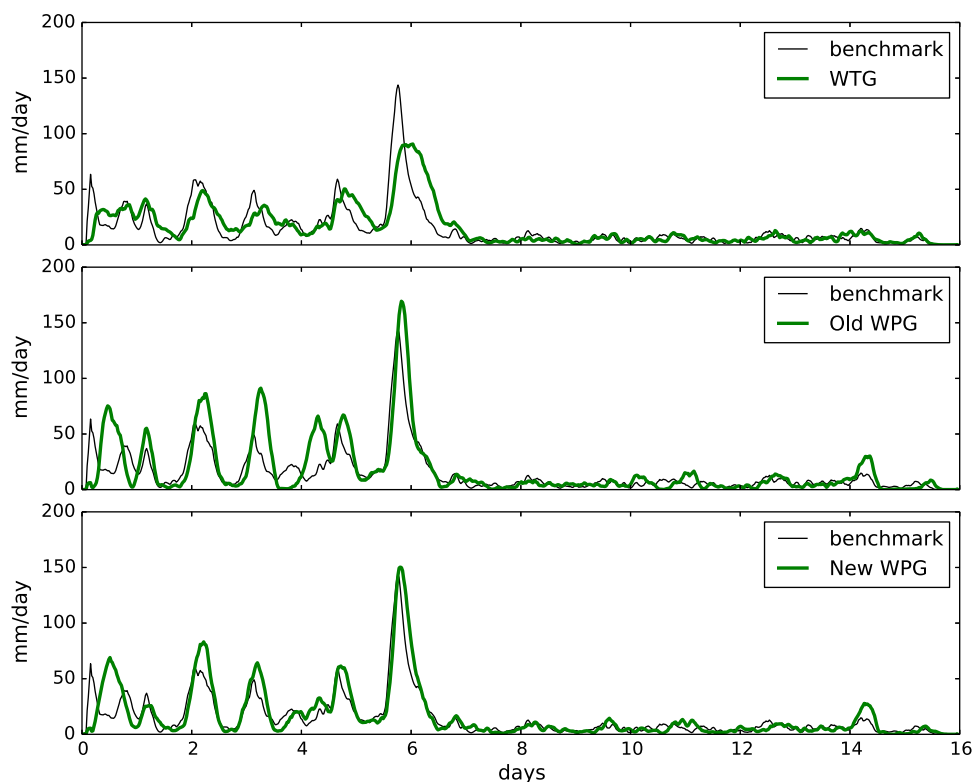


Figure 4. Precipitation time series for the TWP-ICE test case. In all plots, the thin black line is the precipitation rate from the benchmark simulation with prescribed w . The thick green line in the top plot is the precipitation from the simulation coupled to WTG ($\tau = 0.725$ h); the middle and bottom plots show old WPG and new WPG ($L = 128$ km for both), respectively.

shown by the thin black line. By eye, all of the parameterizations perform relatively well throughout the entire 16 day period. More quantitatively, the R^2 values are 0.590, 0.656, and 0.780 for WTG, old WPG, and new WPG, respectively. In the first half of the simulation period, both new WPG and WTG capture the timing and magnitude of the relatively large, almost-daily precipitation events in the benchmark, although the peaks for the WTG case lag the benchmark slightly, and the amplitude of the largest event at the end of day 5 is too small. Old WPG gets the timing of the events roughly correct, but more often than not produces larger amplitudes than the benchmark. In the latter half of the simulation, when the benchmark is characterized by smaller amplitude precipitation events, WTG performs better than either new WPG or old WPG, which both predict more intermittent precipitation in the latter half of the simulation than the benchmark.

4.2. ARM-Southern Great Plains

In addition to the TWP-ICE experiments, we perform tests using a nearly identical model setup and procedure applied to data from the July 1995 intensive observation period (IOP) at the ARM Southern Great Plains (SGP) site [Ghan *et al.*, 1999]. A time-varying radiative cooling profile (from a separate simulation) and time-invariant surface advective tendencies (from observations) are applied as in the TWP-ICE experiments. Because this field site is over land rather than ocean, we prescribe the time-mean of the observed surface fluxes for all SGP simulations. Additionally, for the WPG runs, we apply the same boundary layer linearization used in WTG to reduce the sensitivity to the diurnal cycle of heating.

We do not include the effects of rotation, despite the fact that the ARM SGP site is located at 36.5°N , well outside the tropics. At this latitude, the Rossby deformation radius is ≈ 2000 km, which is an order of magnitude greater than the horizontal extent of the model domain. Thus, we might expect that rotation would not affect the dynamics contained within the model domain, and the assumption of weak temperature and pressure gradients across the model domain and the environment are not grossly violated. Also, convection in the midlatitudes is more strongly forced by large-scale convergence than in the tropics; on these grounds

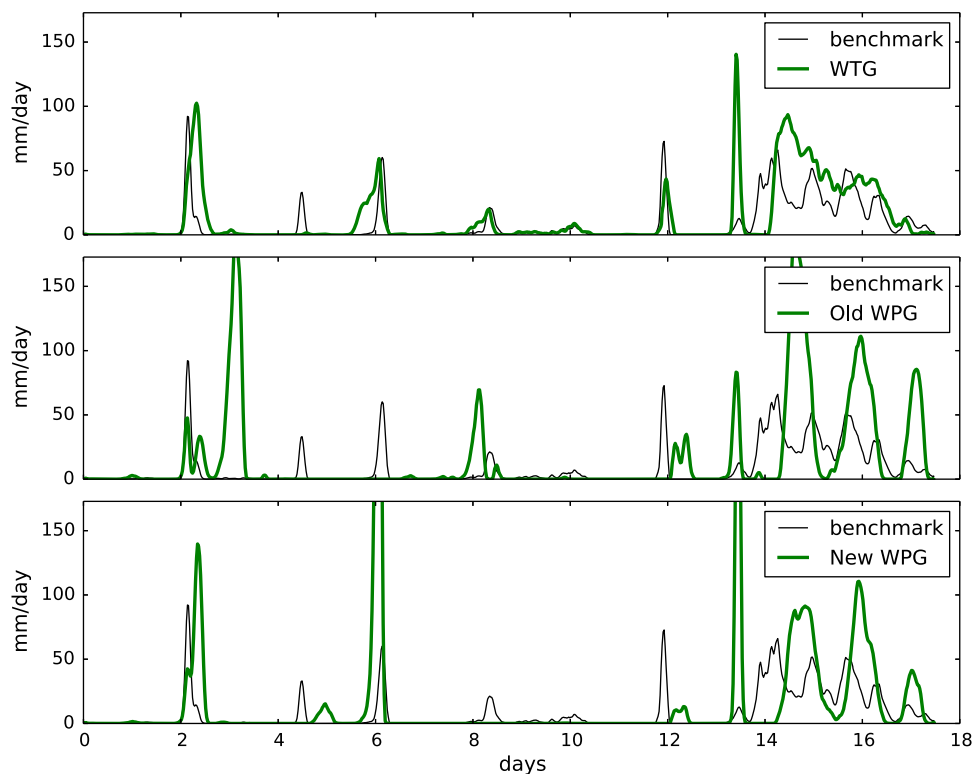


Figure 5. Same as Figure 4, but for the SGP test case. Maximum rainfall rates for the old WPG and new WPG cases are 422 and 365 mm/d, respectively.

we might expect parameterized large-scale dynamics to actually perform better in midlatitudes than in the tropics.

Figure 5 shows the precipitation time series from simulations based on the SGP case using WTG (top), old WPG (middle), and new WPG (bottom). Again, in all three plots, precipitation from the benchmark simulation (forced vertical velocity) is shown by the thin black line.

By eye, we see that WTG outperforms both new and old WPG for this case, although none of the parameterizations perform as well as in the TWP-ICE self-consistency test. The precipitation events in WTG (top, thick red line) are close to the same magnitude as the benchmark, with the exception of the event on day 13, which is spuriously large, and the event on day 4, which is absent. The timing of WTG precipitation events is similar to the benchmark, although some WTG events lead the benchmark by up to 12 h (days 6 and 8) while others lag by a few hours (days 2 and 14). On the other hand, both versions of WPG overpredict the magnitude of almost all precipitation events, and the timing is significantly delayed for the events on days 4, 8, and 12. Furthermore, WTG simulates the persistent rainfall from days 14–16 of the benchmark simulation better than both versions of WPG, which predict almost-daily precipitation events with magnitudes much larger than the benchmark.

4.3. Gravity-Wave Resonance

We performed an additional set of simulations based on the SGP case, similar to the time-varying self-consistency tests described above, but instead using time-varying surface fluxes and interactive radiation for both the benchmark and WTG/WPG-coupled runs. This is still a self-consistency test, as the benchmark and WTG/WPG-coupled runs are subject to the same forcings, but now the SDS scheme must respond to forcings other than column buoyancy anomalies. This framework is perhaps more representative of how WTG and WPG might be used to test CRM's ability to reproduce the properties of the observed atmosphere. One other important difference between these simulations and the SGP simulations described above (and shown in Figure 5) is the use of a moister initial condition, which leads to larger magnitude precipitation

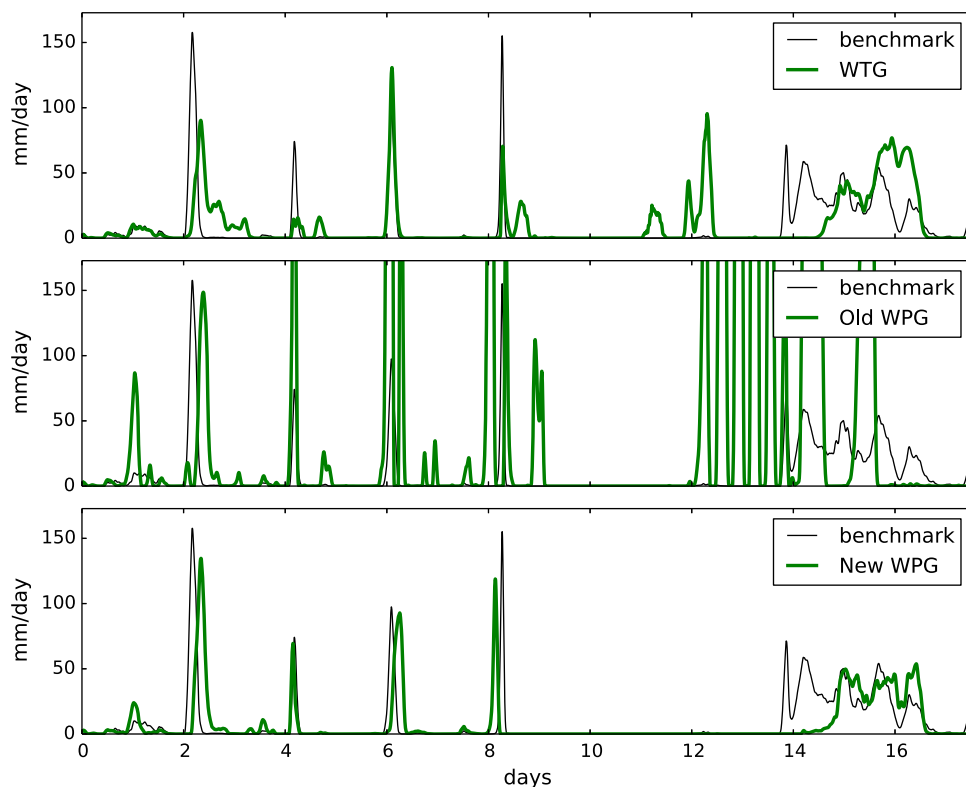


Figure 6. Precipitation time series for the SGP case with interactive radiation and time-varying surface and advective forcings. In all plots, the thin black line is the precipitation rate from the benchmark simulation with prescribed w . The thick green lines in all plots show precipitation from the SDS-coupled runs; in the top plot is the precipitation from the simulation coupled to WTG ($\tau = 0.725$ h); the middle and bottom plots show old WPG and new WPG ($L = 128$ km for both), respectively. Maximum rainfall rate for the old WPG case is 1470 mm/d.

events in the benchmark and coupled simulations, but should not affect the dynamical resonance we explore in this section.

The results of this experiment are shown in Figure 6. Old WPG (middle, orange solid line) clearly performs the worst of the three large-scale dynamics parameterizations, with peak precipitation rates more than twice as large as the benchmark case, and, starting around day 12, a series of large rainfall events seemingly unrelated to anything in the benchmark simulation. These wild oscillations are not present in new WPG, and they are the result of the gravity-wave resonance mentioned earlier.

4.3.1. Why the Resonance?

From the precipitation time series in Figure 6, it is clear that new WPG is a substantial improvement over old WPG. This improvement is due to the improved handling of transient disturbances in new WPG; in particular, new WPG eliminates the spurious gravity-wave resonance in old WPG, as shown by *Edman and Romps* [2014]. The resonance works as follows: a column coupled to old WPG behaves as though a plane wave of wavelength L is passing through the domain; buoyancy anomalies with nearly the same frequency as this wave can trigger a resonance, amplifying the anomaly rather than damping it away. For the shallow-water case considered by *Edman and Romps* [2014], the resonance occurs only at the frequency $f = \omega / (2\pi) = c / (2\pi L)$, where $c = \sqrt{gh}$ is the wave speed in a shallow fluid of depth h . Through a separation of variables, it can be shown that a continuously stratified fluid obeys a set of shallow-water equations, each corresponding to a different “equivalent depth” [e.g., *Matsuno*, 1966]. If one imposes a so-called “rigid lid” somewhere in the atmosphere (i.e., $w \rightarrow 0$ at some z), the vertical structure of the stratified fluid can be decomposed into a discrete set of vertical modes, each with a distinct wave speed c . While perhaps not physically realistic, the rigid lid assumption has been justified in the literature [e.g., *Mapes*, 1998] and is often invoked in studies of tropical circulations [e.g., *Dias et al.*, 1983; *Haertel and Johnson*, 1998; *Tulich et al.*, 2007]. Because the continuously stratified fluid supports a spectrum of wave speeds and vertical structures,

old WPG has the potential for gravity-wave resonance at any of the discrete frequencies $f_i = c_i / (2\pi L)$, where c_i is wave speed of the i th vertical mode.

To see this explicitly, consider the Boussinesq equations linearized about a motionless hydrostatic base state. If we use the old WPG approximation, these equations become

$$\partial_t B = -N^2 w + Q, \tag{9}$$

$$\partial_z p = \rho B, \tag{10}$$

$$\partial_z w = -\delta, \tag{11}$$

$$\partial_t \delta = \frac{1}{\rho} \frac{p}{L^2} - \alpha^* \delta. \tag{12}$$

Here B is the buoyancy, Q is the buoyancy forcing, α^* is a damping term, and δ is the horizontal divergence. Assuming N^2 is constant with height and the dynamics are inviscid ($\alpha^* = 0$), these equations can be reduced to the following equation for the buoyancy:

$$\partial_t^2 \partial_z^2 B - \frac{N^2}{L^2} B = \partial_t \partial_z^2 Q. \tag{13}$$

For a forcing of the form $Q = Q_0 e^{i\omega t + imz}$, where ω is the forcing frequency and m is the vertical wave number, the solutions for B can take the form $B_0 e^{i\omega t + imz}$. Plugging this into equation (13), we find an expression for the amplitude of the buoyancy anomaly B_0 :

$$B_0 = - \frac{im^2 \omega}{m^2 \omega^2 - N^2 / L^2} Q_0. \tag{14}$$

The amplitude B_0 goes to infinity as ω goes to N/mL . Since N/m is the phase speed of a hydrostatic gravity wave with vertical wave number m , we find that the gravity-wave resonance occurs at $f = \omega / (2\pi) = c_m / (2\pi L)$, where c_m is the phase speed of the mode with vertical wave number m . Therefore, we expect that the gravity-wave resonance in old WPG could manifest at a variety of frequencies and with particular vertical structures, corresponding to the vertical modes m and their associated phase speeds c_m .

Edman and Romps [2014] showed that new WPG eliminated this gravity-wave resonance in the shallow-water system. Here we show that new WPG eliminates the gravity-wave resonance in a continuously stratified fluid for any vertical mode. The Boussinesq system for new WPG is:

$$\partial_t B = -N^2 w + Q, \tag{15}$$

$$\partial_z p = \rho B, \tag{16}$$

$$\partial_z w = -\delta, \tag{17}$$

$$\partial_t \delta' = \frac{1}{\rho} \frac{p}{L^2} - \alpha^* \delta', \tag{18}$$

$$\delta = \delta' + \frac{2\pi L}{HN} \partial_t \delta'. \tag{19}$$

The difference between these equations and those for old WPG is the addition of (19), which alters δ by a term proportional to the time for a first-baroclinic mode to propagate across a distance L . This incorporates the effect of the gravity wave back reaction discussed in Edman and Romps [2014].

Reducing these equations to a single equation for the buoyancy in the inviscid case ($\alpha^* = 0$), we get

$$\partial_t^2 \partial_z^2 B - \frac{2\pi N}{HL} \partial_t B - \frac{N^2}{L^2} B = \partial_t \partial_z^2 Q. \tag{20}$$

For an oscillating source $Q = Q_0 e^{i\omega t + imz}$ (where ω and m real and nonzero), we search for solutions of the form $B = B_0 e^{i\omega t + imz}$ and find

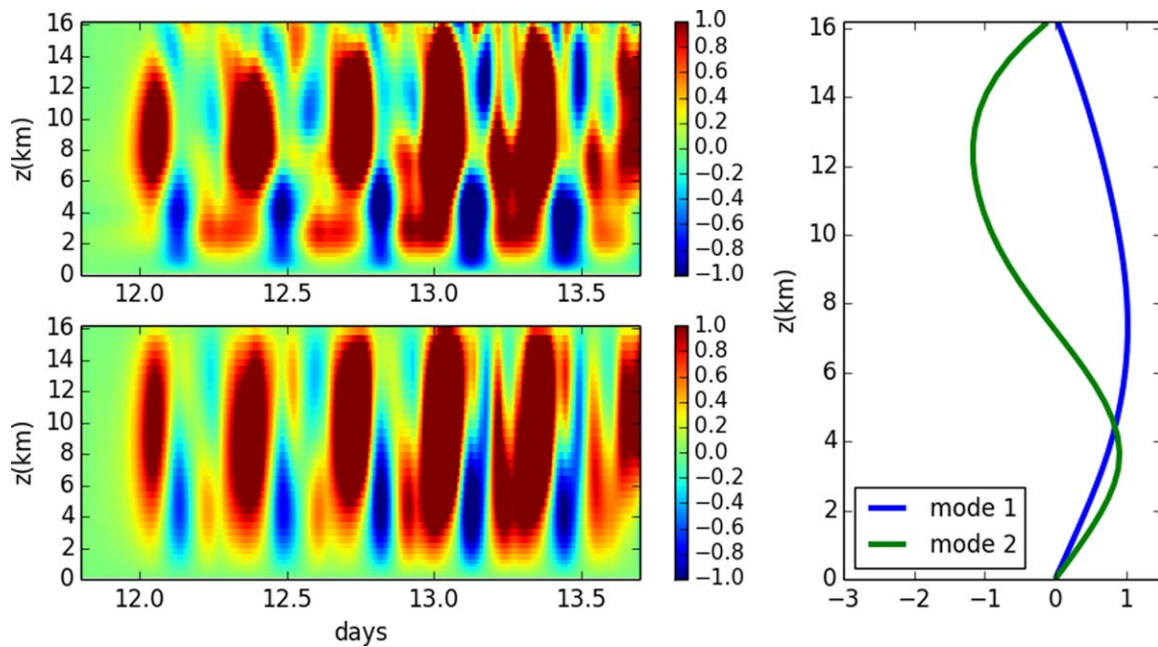


Figure 7. (top) Time series of w from the SGP simulation with interactive radiation and time-varying surface and advective forcings coupled to old WPG. (bottom) Projection of w time series onto the first two vertical modes. (right) First two vertical modes with a rigid lid at the tropopause.

$$B_0 = -\frac{im^2\omega}{m^2\omega^2 - \frac{2\pi N}{HL}i\omega - \frac{N^2}{L^2}}Q_0. \quad (21)$$

Clearly, there is no combination of real m and real ω that can make the denominator zero. Therefore, there is no resonance for any forcing—i.e., for any frequency and vertical wave number—in new WPG.

4.3.2. Vertical Mode Decomposition

In the above example using constant N^2 , the sine functions form an orthogonal basis with which we can expand any vertical profile. For the general case of $N^2(z)$, we can define a set of vertical modes by solving the vertical structure equation,

$$\frac{d^2W(z)}{dz^2} + \frac{N^2(z)}{c_m^2}W(z) = 0, \quad (22)$$

where $W(z)$ is the vertical structure function for w . Subject to boundary conditions $w = 0$ at the surface and the tropopause, this produces a set of orthogonal eigenfunctions corresponding to discrete wave speeds c_m .

We perform this decomposition for the SGP simulation coupled to old WPG using the mean $N^2(z)$ and placing a rigid lid at the cold-point tropopause ($z = 16.4$ km). The first two vertical modes are plotted on the right side of Figure 7. To gain some insight into the wild oscillations beginning around day 12 of the old WPG simulation, we project the vertical profile of w (averaged every 5 minutes) onto these vertical modes; the result is the bottom left of Figure 7. Compared to the actual w time series from the simulation (top left), the first two modes capture the basic features of the oscillation: a shallow (mode 2) circulation leads a deeper (mode 1) circulation, with a frequency of approximately 4 cycles/day.

The top plot of Figure 8 shows the time series of projection coefficients for each of the first four vertical modes. Clearly, most of the amplitude is contained in the first three modes. The bottom plot shows the power spectra of the projection coefficients for the first four vertical modes; the x axis is rescaled by the factor $2\pi L$ such that it is in units of wave speed. The vertical black lines correspond to the wave speeds of the different vertical modes, e.g., $c_1 = 55.2$ m s⁻¹ and $c_2 = 28.2$ m s⁻¹. If the oscillations are indeed caused by the gravity-wave resonance in old WPG, then we expect the peaks in the power spectra to align with one or

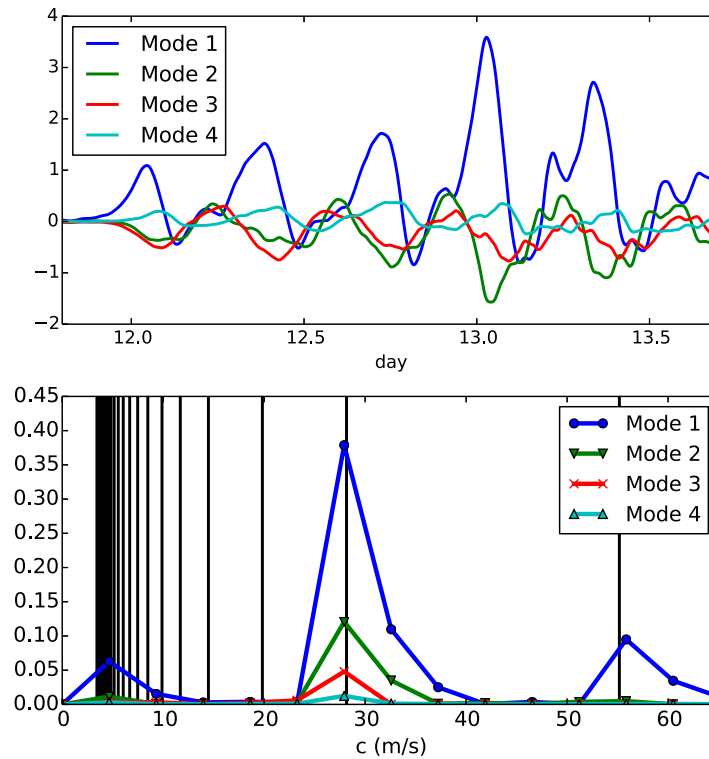


Figure 8. (top) Time series of projection coefficient for the first four vertical normal modes. (bottom) Power spectra for the time series of projection coefficients for the first four vertical modes. The x axis has been rescaled to be in units of wave speed; the black vertical lines correspond to the wave speeds of the vertical modes.

more of these vertical lines. The strongest peak for all modes occurs at c_2 , the resonance we would associate with the vertical structure of mode 2. This is consistent with the behavior in Figure 7, where the mode 2 circulation appears to trigger the deeper circulation, causing them to oscillate at the same frequency. Mode 1 also has a peak near $c_1 = 55.2 \text{ m s}^{-1}$ and another around 5 m s^{-1} ; the peak at c_1 is due to gravity-wave resonance with a mode-1 vertical structure, while the peak near 5 m s^{-1} appears to be associated with higher vertical modes.

5. Discussion

In this study, we have evaluated three methods for parameterizing large-scale dynamics (SDS schemes) in CRMs, using a self-consistency framework designed to isolate errors introduced by the SDS

scheme from errors in the convection simulated by the CRM. WTG, old WPG, and new WPG all pass RCE self-consistency tests for large τ and L (large-scale environment weakly coupled to the column) and for small τ and L (large-scale environment strongly coupled to the column). For intermediate L , however, old WPG and new WPG exhibit domain-mean descent that is comparable to the radiatively driven clear-sky descent and, therefore, do not pass this part of the self-consistency test.

These mixed results do not necessarily doom the enterprise of parameterizing large-scale dynamics. One notable limitation of the versions of WPG and WTG considered here is that they rely on a single parameter related to the wave speed of a particular baroclinic mode (τ in WTG, $2\pi/\text{HN}$ in new WPG); others have suggested that a spectral decomposition approach might be the best way forward [Bergman and Sardeshmukh, 2004; Mapes, 2004]. Herman and Raymond [2014] recently introduced a “spectral WTG” based on this approach, and new WPG could be extended to a spectral framework as well.

The secondary goal of this study is to evaluate the new form of WPG introduced in Edman and Romps [2014], and confirm that it represents a significant advance over prior implementations of WPG. We find that, in a self-consistency test based on observations from TWP-ICE, new WPG simulates the benchmark precipitation time series better than old WPG and WTG, but in a test based on observations from the ARM SGP site, both versions of WPG perform poorly, and WTG performs better than either version WPG.

We also show the traditional version of WPG [e.g., Romps, 2012b] is prone to a potentially troublesome gravity-wave resonance, where buoyancy anomalies near the natural frequency of the column are amplified rather than damped away. In another set of self-consistency tests based on the ARM SGP observations (Figure 6), which use interactive radiation and time-varying surface and advective forcings, we find that old WPG is severely affected by this gravity-wave resonance, and that the new version of WPG eliminates this resonance and simulates precipitation time series better than old WPG. As a result, we find that this gravity-wave resonance can pose a significant problem in observationally based experiments, but we confirm the new version of WPG does not suffer from this deficiency.

Acknowledgments

This work was supported by the U.S. Department of Energy's Earth System Modeling an Office of Science, Office of Biological and Environmental Research program under contract DE-AC02-05CH11231, as well as the National Science Foundation Graduate Research Fellowship under grant DGE 1106400. Numerical simulations were performed on the Lawrence cluster provided by the IT Division at the Lawrence Berkeley National Laboratory and the Hopper cluster provided by the National Energy Research Scientific Computing Center, both of which are supported by the Office of Science of the U.S. Department of Energy under contract DE-AC02-05CH11231. Simulation results and forcing data from SGP and TWP-ICE used in this paper, as well as Python code for the vertical mode decomposition, are available from Jacob Edman (jedman@berkeley.edu) upon request. We also thank two anonymous reviewers for their helpful comments.

References

- Bergman, J. W., and P. D. Sardeshmukh (2004), Dynamic stabilization of atmospheric single column models, *J. Clim.*, *17*(5), 1004–1021, doi:10.1175/1520-0442(2004)017<1004:DSOASC>2.0.CO;2.
- Blossey, P. N., C. S. Bretherton, and M. C. Wyant (2009), Subtropical low cloud response to a warmer climate in a superparameterized climate model. Part II: Column modeling with a cloud resolving model, *J. Adv. Model. Earth Syst.*, *2*, 8, doi:10.3894/JAMES.2009.1.8.
- Bony, S., G. Bellon, D. Klocke, S. Sherwood, S. Fermepin, and S. Denvil (2013), Robust direct effect of carbon dioxide on tropical circulation and regional precipitation, *Nat. Geosci.*, *6*(6), 447–451, doi:10.1038/ngeo1799.
- Bretherton, C. S., P. N. Blossey, and M. Khairoutdinov (2005), An energy-balance analysis of deep convective self-aggregation above uniform SST, *J. Atmos. Sci.*, *62*(12), 4273–4292.
- Chiang, J., and A. Sobel (2002), Tropical tropospheric temperature variations caused by ENSO and their influence on the remote tropical climate*, *J. Clim.*, *15*, 2616–2631.
- Cohen, B. G., and G. C. Craig (2004), The response time of a convective cloud ensemble to a change in forcing, *Q. J. R. Meteorol. Soc.*, *130*(598), 933–944, doi:10.1256/qj.02.218.
- Daleu, C. L., S. J. Woolnough, and R. S. Plant (2012), Cloud-resolving model simulations with one- and two-way couplings via the weak temperature gradient approximation, *J. Atmos. Sci.*, *69*(12), 3683–3699, doi:10.1175/JAS-D-12-058.1.
- Dias, P. S., W. Schubert, and M. DeMaria (1983), Large-scale response of the Tropical Atmosphere to Transient Convection, *J. Atmos. Sci.*, *40*, 2689–2707.
- Edman, J. P., and D. M. Romps (2014), An improved weak pressure gradient scheme for single-column modeling, *J. Atmos. Sci.*, *71*(7), 2415–2429, doi:10.1175/JAS-D-13-0327.1.
- Emanuel, K., and A. Sobel (2013), Response of tropical sea surface temperature, precipitation, and tropical cyclone-related variables to changes in global and local forcing, *J. Adv. Model. Earth Syst.*, *5*, 447–458, doi:10.1002/jame.20032.
- Emanuel, K., A. A. Wing, and E. M. Vincent (2014), Radiative-convective instability, *J. Adv. Model. Earth Syst.*, *6*, 75–90, doi:10.1002/2013MS000270.
- Fridlind, A., A. Ackerman, J. Petch, and P. Field (2010), ARM/GCSS/SPARC/TWP-ICE CRM intercomparison study, *Tech. Rep. NASA-TM-2010-215858*, Natl. Aeronaut. and Space Admin, Greenbelt, Md.
- Ghan, S. J., D. A. Randall, K. Xu, and D. G. Cripe (1999), An intercomparison of single-column model simulations of summertime midlatitude continental convection, paper presented at Ninth ARM Science Team Meeting Proceedings, Department of Energy, San Antonio, Tex.
- Haertel, P., and R. Johnson (1998), Two-day disturbances in the equatorial western Pacific, *Q. J. R. Meteorol. Soc.*, *124*, 615–636.
- Held, I. M., R. S. Hemler, and V. Ramaswamy (1993), Radiative-convective equilibrium with explicit two-dimensional moist convection, *J. Atmos. Sci.*, *50*(23), 3909–3927.
- Herman, M. J., and D. J. Raymond (2014), WTG cloud modeling with spectral decomposition of heating, *J. Adv. Model. Earth Syst.*, 1121–1140, doi:10.1002/2014MS000359.
- Holton, J. (1973), A one-dimensional cumulus model including pressure perturbations, *Mon. Weather Rev.* *101*(3), 201–205.
- Jeevanjee, N., and D. M. Romps (2013), Convective self-aggregation, cold pools, and domain size, *Geophys. Res. Lett.*, *40*, 1–5, doi:10.1002/grl.50204.
- Kuang, Z. (2008), Modeling the interaction between cumulus convection and linear gravity waves using a limited-domain cloud system resolving model, *J. Atmos. Sci.*, *65*(2), 576–591, doi:10.1175/2007JAS2399.1.
- Kuang, Z. (2011), The wavelength dependence of the gross moist stability and the scale selection in the instability of column-integrated moist static energy, *J. Atmos. Sci.*, *68*(1), 61–74, doi:10.1175/2010JAS3591.1.
- Kuang, Z. (2012), Weakly forced mock walker cells, *J. Atmos. Sci.*, *69*(9), 2759–2786, doi:10.1175/JAS-D-11-0307.1.
- Mapes, B. (1998), The large-scale part of tropical mesoscale convective system circulations: A linear vertical spectral band model, *J. Meteorol. Soc. Jpn.*, *76*(1), 29–55.
- Mapes, B. (2004), Sensitivities of cumulus-ensemble rainfall in a cloud-resolving model with parameterized large-scale dynamics, *J. Atmos. Sci.*, *61*, 2308–2317.
- Matsuno, T. (1966), Quasi-geostrophic motions in the equatorial area, *J. Meteorol. Soc. Jpn.*, *44*(1), 25–43.
- Muller, C. J., and I. M. Held (2012), Detailed investigation of the self-aggregation of convection in cloud-resolving simulations, *J. Atmos. Sci.*, *69*(8), 2551–2565.
- Nilsson, J., and K. Emanuel (1999), Equilibrium atmospheres of a two-column radiative-convective model, *Q. J. R. Meteorol. Soc.*, *125*, 2239–2264.
- Raymond, D. (2007), Testing a cumulus parameterization with a cumulus ensemble model in weak-temperature-gradient mode, *Q. J. R. Meteorol. Soc.*, *1085*, 1073–1085, doi:10.1002/qj.80.
- Raymond, D. J., and X. Zeng (2000), Instability and large-scale circulations in a two-column model of the tropical troposphere, *Q. J. R. Meteorol. Soc.*, *126*, 3117–3135.
- Raymond, D. J., and X. Zeng (2005), Modelling tropical atmospheric convection in the context of the weak temperature gradient approximation, *Q. J. R. Meteorol. Soc.*, *131*(608), 1301–1320, doi:10.1256/qj.03.97.
- Romps, D. M. (2008), The dry-entropy budget of a moist atmosphere, *J. Atmos. Sci.*, *65*(12), 3779–3799, doi:10.1175/2008JAS2679.1.
- Romps, D. M. (2012a), Weak pressure gradient approximation and its analytical solutions, *J. Atmos. Sci.*, *69*(9), 2835–2845, doi:10.1175/JAS-D-11-0336.1.
- Romps, D. M. (2012b), Numerical tests of the weak pressure gradient approximation, *J. Atmos. Sci.*, *69*(9), 2846–2856, doi:10.1175/JAS-D-11-0337.1.
- Sessions, S. L., S. Sugaya, D. J. Raymond, and A. H. Sobel (2010), Multiple equilibria in a cloud-resolving model using the weak temperature gradient approximation, *J. Geophys. Res.*, *115*, D12110, doi:10.1029/2009JD013376.
- Sobel, A., and C. Bretherton (2000), Modeling tropical precipitation in a single column, *J. Clim.*, *13*, 4378–4392.
- Sobel, A., G. Bellon, and J. Bacmeister (2007), Multiple equilibria in a single column model of the tropical atmosphere, *Geophys. Res. Lett.*, *34*, L22804, doi:10.1029/2007GL031320.
- Stephens, G. L., S. van den Heever, and L. Pakula (2008), Radiative-convective feedbacks in idealized states of radiative-convective equilibrium, *J. Atmos. Sci.*, *65*(12), 3899–3916.
- Tulich, S. N., D. A. Randall, and B. E. Mapes (2007), Vertical-mode and cloud decomposition of large-scale convectively coupled gravity waves in a two-dimensional cloud-resolving model, *J. Atmos. Sci.*, *64*(4), 1210–1229, doi:10.1175/JAS3884.1.
- Wang, S., and A. Sobel (2012), Impact of imposed drying on deep convection in a cloud-resolving model, *J. Geophys. Res.*, *117*, D02112, doi:10.1029/2011JD016847.

- Wang, S., and A. H. Sobel (2011), Response of convection to relative sea surface temperature: Cloud-resolving simulations in two and three dimensions, *J. Geophys. Res.*, *116*, D11119, doi:10.1029/2010JD015347.
- Wang, S., A. Sobel, and Z. Kuang (2013), Cloud-resolving simulation of TOGA-COARE using parameterized large-scale dynamics, *J. Geophys. Res. Atmos.*, *118*, 6290–6301, doi:10.1002/jgrd.50510.
- Wing, A. A., and K. A. Emanuel (2014), Physical mechanisms controlling self-aggregation of convection in idealized numerical modeling simulations, *J. Adv. Model. Earth Syst.*, *6*, 59–74, doi:10.1002/2013MS000269.